

# Flash and Breakdown: Thermal Runaway and Dielectric Breakdown as Competing Mechanisms During Flash Sintering of Barium Titanate

Daniil Lewin,\* Ivo Michiels, Sobhan Mohammadi Fathabad, Eva Kröll, Karl-Heinz Menze, and Doru C. Lupascu

Herein, hot-spot generation in bulk barium titanate samples is investigated during controlled current ramping at various rates using *in situ* dilatometry. The incubation of the flash event is separated from dielectric breakdown at high current densities, which has previously been attributed to cause flash incubation in barium titanate. The lower boundary of the onset temperature of the flash event in barium titanate is investigated through conventional flash experiments at high electric fields. Despite incubating through thermal runaway, the lower boundary does not coincide with the Debye temperature of barium titanate.

## 1. Introduction

Upscaling of flash sintering is one of the two major challenges commonly associated with this novel densification technique for ceramics.<sup>[1,2]</sup> Flash sintering distinguishes itself from established field-assisted methods like field assisted sintering technique/spark plasma sintering (FAST/SPS) as well as new methods like ultrafast high-temperature sintering, due to the electric current passing exclusively through the green body at all times.<sup>[3,4]</sup> In theory, this should make flash sintering more viable for upscaling than the aforementioned methods or other novel methods like black-light sintering that apply heat energy to the surface of the sample.<sup>[5]</sup> In reality, upscaling is strongly limited due to the formation of preferential current paths commonly referred to as hot spots.<sup>[2,6,7]</sup> Among the oxides most investigated for flash sintering, barium titanate demonstrates an especially strong case

of inhomogeneities due to hot-spot formation. Studies report tunnel-shaped damage piercing through the sample rather than the uneven distribution of density and grain sizes commonly reported for other materials. Even further, the parameters at which such damage occurs change significantly between studies: values between 12 and 75 mA mm<sup>-2</sup> have been reported for conventional flash experiments.<sup>[8,9]</sup> This seeming contradiction is partly explained by the variation of sample geometry: ever since the initial study by Cologna et al., the dog-bone-shaped green body has estab-

lished itself as the sample geometry of flash sintering.<sup>[10]</sup> Such green bodies typically have a length of 20–30 mm between the electrodes and a cross section of roughly 3 × 1.5 mm. The wire electrodes which contact the samples are also used to suspend the green body in the oven ultimately minimizing the contact area between the sample and other parts of the setup. Specifically for such a geometry, a lot of progress with regard to the quality of the sintered ceramics has been made. In the case of barium titanate, the initial study utilizing conventional flash sintering has already reached a high density of the samples, while a recent study utilizing the novel controlled current ramping method has achieved great homogeneity and grain-size control.<sup>[9,11]</sup> These results are in strong contrast to studies conducted on shorter samples with a bigger cross-section (5 × 5 mm) reporting far lower densities and damage to the samples and concluding that conventional flash sintering should be avoided for barium titanate.<sup>[8,12]</sup>

In a previous study, we investigated samples of different sizes using *in situ* infrared imaging and observed a strong decrease in temperature differences for thinner samples.<sup>[13]</sup> Another finding of our study was that controlled current ramping efficiently decreases temperature gradients, which is in line with the overall reported increase in homogeneity.<sup>[14–17]</sup>

In the present study, we apply the controlled current ramping method to bulk barium titanate samples with the aim of avoiding hot-spot formation. We vary the ramping rates as well as modify our setup specifically to create strong, inhomogeneous thermal conduction away from the samples to observe the effect on the hot-spot appearance. A recent study by Mishra et al. has determined the Debye temperature as the boundary which is approached at high fields for the onset temperature of the flash event for gadolinium-doped ceria (GDZ), yttria-stabilized zirconia (YSZ), and TiO<sub>2</sub>.<sup>[18]</sup> Additionally, in their study, any onset

D. Lewin, I. Michiels, S. M. Fathabad, E. Kröll, K.-H. Menze, D. C. Lupascu  
Institute for Materials Science and Center for Nanointegration Duisburg-Essen (CENIDE)  
University of Duisburg-Essen  
Universitätsstrasse 15, 45141 Essen, Germany  
E-mail: daniil.lewin@uni-due.de

 The ORCID identification number(s) for the author(s) of this article can be found under <https://doi.org/10.1002/adem.202300142>.

© 2023 The Authors. Advanced Engineering Materials published by Wiley-VCH GmbH. This is an open access article under the terms of the Creative Commons Attribution-NonCommercial-NoDerivs License, which permits use and distribution in any medium, provided the original work is properly cited, the use is non-commercial and no modifications or adaptations are made.

DOI: [10.1002/adem.202300142](https://doi.org/10.1002/adem.202300142)

variation due to different green-body grain sizes disappears for higher fields merging the individual curves toward the Debye-temperature barrier. To further investigate the onset of flash in barium titanate, we conduct a similar study with high electric fields to find the lower boundary for the breakdown while varying the sample geometry and the setup.

## 2. Results and Discussion

**Figure 1** depicts an example for the typical data set for each experiment: the linear shrinkage of the green body, the power density, and the applied electric field. As the current strength is linearly increased throughout the experiments, the electric field data is a derivative of the power density, yet it is helpful to highlight changes throughout the experiment. It must also be stated that power density is a purely nominal value, especially when a hot-spot breakdown takes place.

First, at low current values, a power surge occurs, which is best visible in the electric field data. This is directly mirrored in the dilatometry data, as during this time, the sample is thermally expanding. As these peaks transition into a steady decrease of the electric field (yet an overall steady increase in power density), the thermal expansion is replaced by a rapid densification of the sample as seen from the dilatometry data. In absence of an uncontrolled exponential thermal runaway, this can be seen as the onset of the flash event for the current ramping method. In the next section, the power is steadily increasing while the electric field mostly declines. Inflection points in the power density are always mirrored by a change in densification rate recorded by dilatometry. In the final section, a sudden drop in power density appears and is followed by unsteady changes for the remainder of the experiment. Its effect on the dilatometry data is, at first, a significant decrease in densification rate, often followed by a sudden increase in sample length. This increase is different between individual experiments and irreversible, and appears due to damage to the sample.

**Figure 2** depicts datasets for different current ramping rates of 0.125, 0.25, 0.5, and  $1 \text{ mA s}^{-1}$ . We use current density rather than time as the  $x$ -axis to allow for direct data comparison. The voltage peak at the start of the experiment is more pronounced for high current ramping rates, which means a bigger power surge at the start of the experiment. This is somewhat represented by a weak trend of a higher thermal expansion during this power surge. Based on voltage data, this onset of the flash event appears at  $0.72 \pm 0.08 \text{ mA mm}^{-2}$  regardless the ramping rate. For conventional flash experiments, rapid densification based on a steplike current increase is commonly referred to as the actual flash sintering, while a steady densification at elevated current densities is clearly separated as a densification mechanism and commonly referred to as simply field-assisted sintering. Despite having a significant time advantage, the total linear shrinkage throughout the experiment does not vary much between the different current ramping rates. A shrinking rate of  $1.36 \pm 0.15 \text{ \% per mA mm}^{-2}$  is typical for the densification rate as an average and no trend can be observed between ramping rates.

Due to the dependence on current strength rather than time, it can be concluded that the flash sintering process is the dominant mechanism of the densification in the presented data. A steadier,

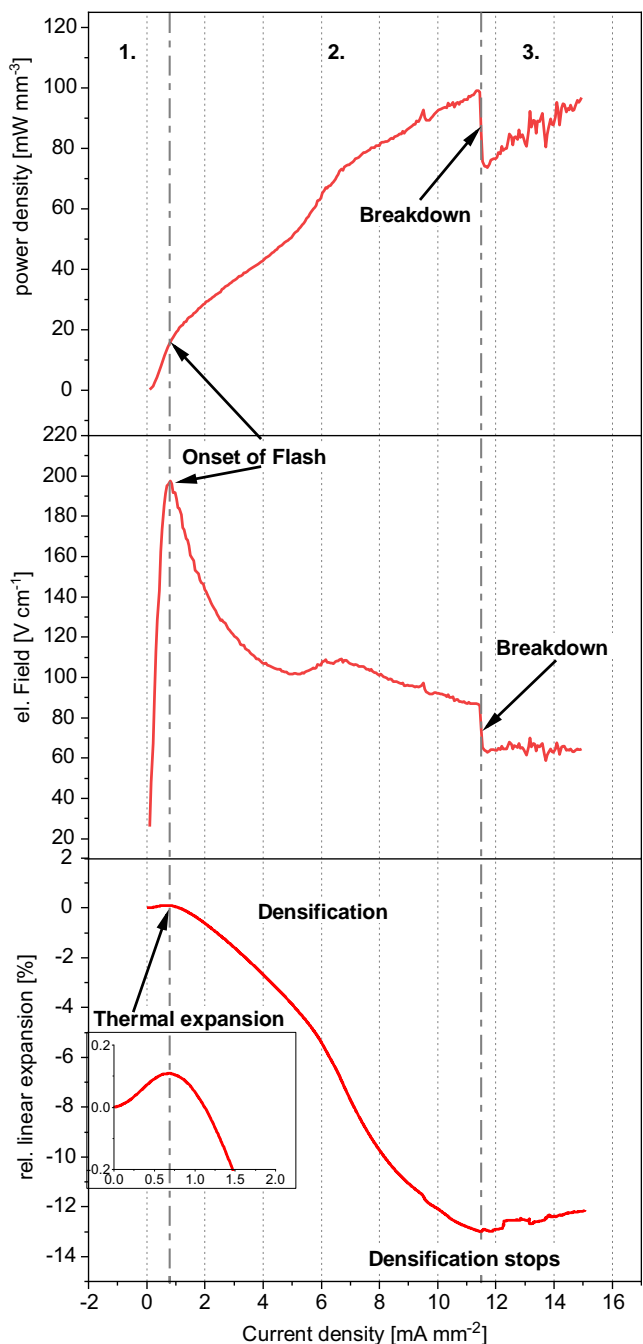


**Figure 1.** Power density, electric field, and relative linear shrinkage, where 1) is incubation of the flash event, 2) is the proper flash event, and 3) is following a critical breakdown.

linear shrinkage rate as well as a significantly lower power surge during incubation at the start of the experiment fully support the commonly reported observation of higher homogeneity for slow ramping rates. As we have shown in our previous study, rapid heating rates cause a bigger temperature difference on the sample surface, meaning a stronger temperature gradient throughout the sample during the flash event and therefore less homogenous results.<sup>[13]</sup>

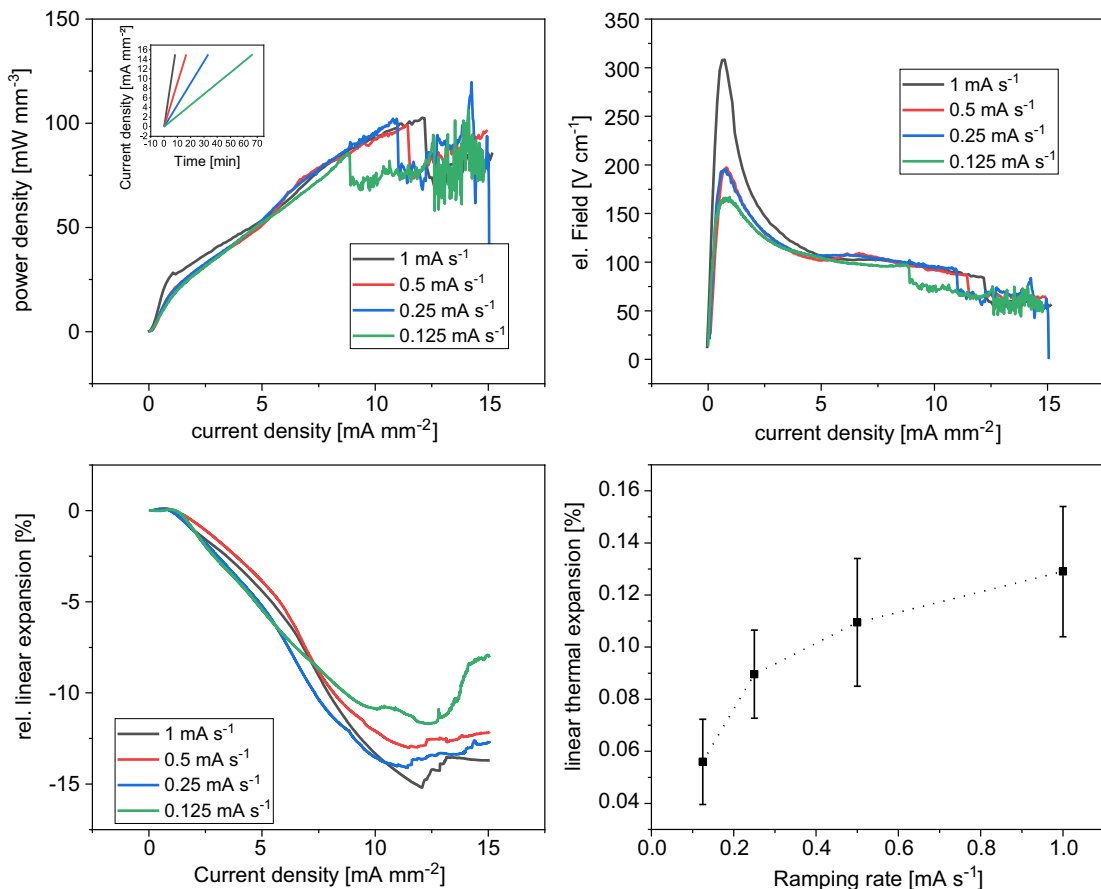


**Figure 2.** Power density (top left), applied electric field (top right) and relative linear shrinkage (bottom left) during controlled current ramping for different ramping rates. A small thermal expansion appears in all experiments, with its magnitude decreasing with slower ramping rates (bottom right).

However, the expected positive effect of the slow, controlled ramping rate does not extend to the appearance of hot-spot breakdowns observed for all experiments within the  $15 \text{ mA mm}^{-2}$  (500 mA) range. Out of twenty experiments for this series, three

strongly deviate from Figure 1 and 2 and experience much earlier breakdown than the other samples. The other measurements form a trend of breakdowns at higher current densities for faster ramping rates, as shown in Figure 3. This is in direct contrast to

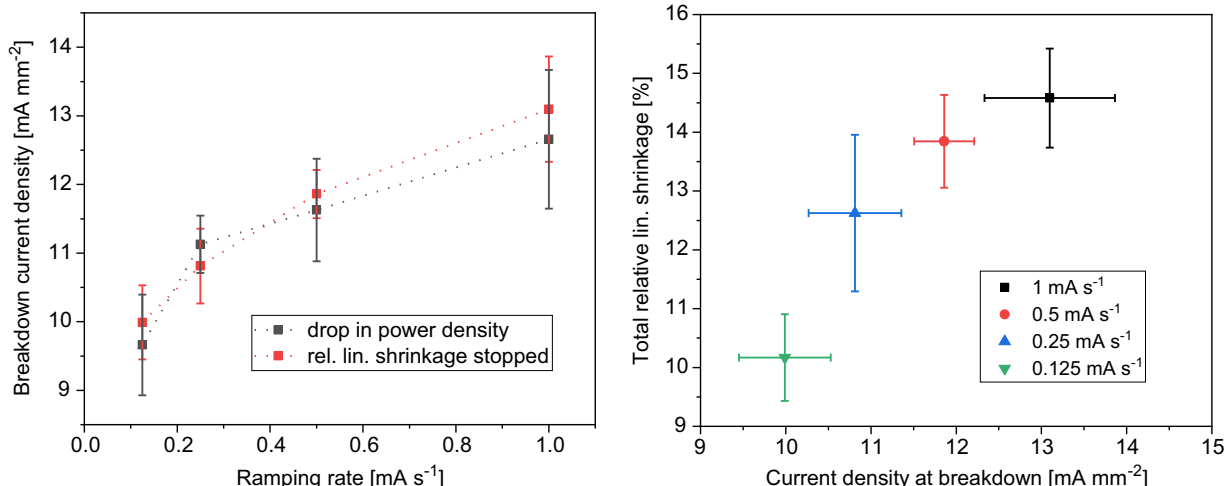


**Figure 3.** Left: initial thermal expansion of the samples before flash onset for different ramping rates. Right: total shrinkage of the sample for different ramping rates with respect to the current density of the breakdown.

the expected behavior. As the densification process of all samples is interrupted by such breakdown at relatively low current density values, the total linear shrinkage appears lower for slower ramping rates.

To secure whether temperature inhomogeneities affect this critical breakdown at all, analogous experiments only for a ramping rate of  $0.5 \text{ mA s}^{-1}$  were performed in a second configuration with the alumina pushrod and alumina wall of the dilatometer not separated from the electrodes by the insets. This configuration is asymmetrical and highly inhomogeneous, as the pushrod has a much smaller diameter than the electrodes and the contact and thermal conduction is different for both sides. Throughout the course of an experiment, this setup configuration drains roughly 10% additional power via the additional heat conduction from the direct alumina contacts instead of the highly porous  $\text{Y}_2\text{O}_3$  freeze-cast insets. The breakdown current density for these experiments is  $10.2 \text{ mA mm}^{-2}$ , a clear decrease.

The commonly described cause for hot-spot formation during flash is the thermal runaway causing an inhomogeneous heating of the sample, in turn causing an inhomogeneous current flow feeding back into the inhomogeneous heat distribution.<sup>[2]</sup> This is clearly the dominant process for the second example, as for all experiments of the series, the thermal hot spot and breakdown happen in the same area, away from the alumina pushrod: the inherent inhomogeneity of the setup causes a thermal hot spot here first. At a certain point, an electric breakdown appears in this location, further exacerbating the current localization. A cross section of such an inhomogeneous sample with a characteristic black colorization at the current path attributed to chemical reduction is pictured in **Figure 4**.<sup>[19]</sup>

However, for the experiments done with different ramping rates, a dielectric breakdown based on a conventional hot-spot formation is unlikely, as slow ramping rates are specifically known to strongly diminish conventional hot-spot patterns across all studies, which is also backed by our data. For the controlled current ramping experiments, the initial onset of the densification process and the critical hot spot are clearly separated. From these observations, we conclude that during flash sintering of barium titanate, we commonly observe two separate events based on different mechanisms: first, a proper flash event usually referenced as a thermal runaway, and later a secondary dielectric breakdown, which in spite of the controlled mode that appears steplike. While the two mechanisms influence each other, as demonstrated by the highly inhomogeneous setup configuration, their causes must be different.

Barium titanate is partly transparent under visible light, making pores directly below the sample surface visible as well. In the direct proximity of the current path, a highly porous structure can be observed (Figure 4), which becomes strongly affected by photoelasticity under polarized light due to internal stresses. Such stresses, typically derived from rapid cooling of a molten material, match the overall appearance of the area as molten during the flash event. This would require a local temperature of at least  $1620^\circ\text{C}$ . The microstructure and grain-size distributions are shown in **Figure 5**: a low density and grain growth appear in the outside layers of the sample. Properly densified and significantly grown grains appear in the bulk of the sample where damage from the dielectric discharge did not occur. Around the breakdown current path indication of melting and solidification can be found. This area includes tightly packed smaller grains,

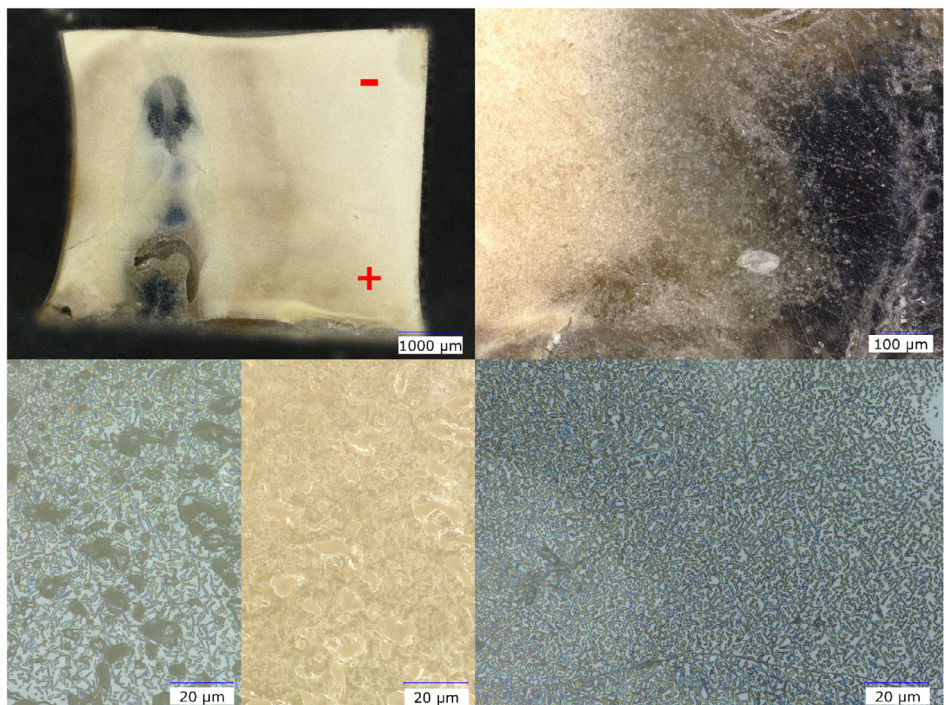


**Figure 4.** Top left: cross section of barium titanate sample after breakdown. Top right: dark area of the hotspot path, adjacent to well-densified material and barely densified material outside. Bottom left: material directly adjacent to the reduced area under polarized and unpolarized light. Big regular pores are mixed with strongly photoelastic inclusions. Bottom right: dense inclusion area on the other side of the preferential current path with no regular pores.

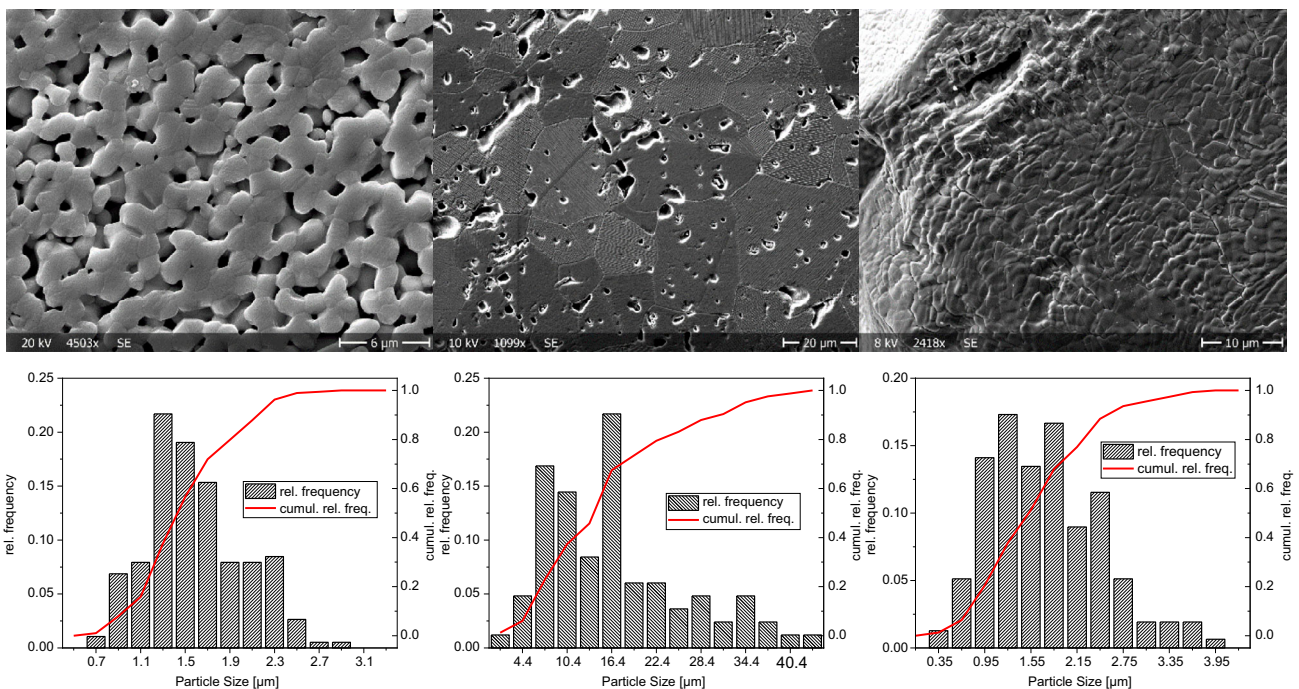


**Figure 5.** Partly sintered grains at the outside layer of the sample (left), properly sintered grains in the bulk of the sample (middle) and grains that formed after melting at the breakdown area (right) and their distributions for the ramping rate of  $0.5 \text{ mA s}^{-1}$ .

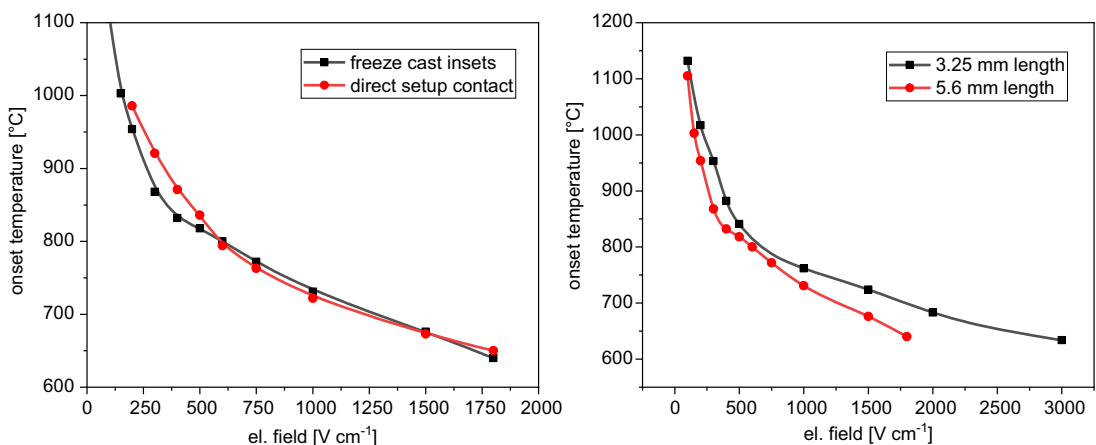


**Figure 6.** Onset temperatures in respect to the electric field for different setup configurations and different sample lengths.

which hints at fast nucleation of molten material, which is in agreement with the fast cooling rates at the end of the flash experiment.

Lastly, **Figure 6** summarizes the onset temperatures of conventional flash-sintering experiments for high electric fields. According to literature, the Debye temperature of barium titanate is roughly at  $200^\circ\text{C}$ , yet all of our measurement series approach much higher values.<sup>[20,21]</sup> In their study, Mishra et al. describe the samples to shatter at high fields, yet in our case, we only observe a very narrow tunnel-shaped damage through one spot of the sample before the current limit is reached with no observable changes to the sample otherwise. For electric fields of  $1500 \text{ V cm}^{-1}$  and above, the location of the breakdown reliably

appears on the outer surface of the sample instead, leaving behind a molten path. Such behavior is more typical for a dielectric breakdown due to the sharp edges of the electrodes forming a singularity, while a thermal hot spot typically incubates in the middle of the sample. In all cases, the dilatometry registers a reversible thermal expansion (and no densification for high fields) before the dielectric breakdown takes place. The current strength steadily increases to at least  $0.6 \text{ mA mm}^{-2}$  before the runaway/breakdown takes place. For a field of  $1500 \text{ V cm}^{-1}$ , this means a nominal power density of at least  $90 \text{ mW mm}^{-3}$ , which is very close to the values we observed during the controlled current ramping before dielectric breakdown. Overall, this demonstrates that even at high fields any type of breakdown

is clearly preceded by a very sharp thermal runaway before a dielectric breakdown, signified by blackening on the anode side, appears.

When comparing different setup configurations, we observe an expected pattern—for lower fields, there is a clear difference in onset temperature, which mostly disappears for higher fields. For samples of different lengths, however, the curves do not converge for high fields. As we have exhausted the voltage limit of our power supply, we cannot presently investigate, whether this gap closes for even higher fields.

Through current ramping, we have clearly separated the onset of the flash event and the densification from the avalanche-like dielectric breakdown at higher current densities. So far, we have only observed this effect in barium titanate. In all cases, we first observed either a stable increase in power density through the sample or a proper thermal runaway before such breakdown was triggered. This strongly suggests that a certain temperature of the samples must be reached before the discharge. In case of our closed dilatometry setup, we cannot conduct IR or black-body radiation measurements, but in our previous study, we have observed several breakdowns in barium titanate during current ramping using an IR camera.<sup>[13]</sup> From that data, the sample temperature at the breakdown can be estimated as roughly 1200 °C. However, the dielectric breakdown appears at a lower power density for samples at lower current ramping rates. This means that the breakdown does not depend on simply reaching a critical temperature inside the samples. Instead, some effect incubating over time must be involved. This can be either due the flash mechanism itself or due to an undetected measurement artifact.

Another feature that must be addressed is the inflection points in power density during the densification. As is best visible in the electric field data in Figure 1, there is an inflection point for the power density at  $5 \text{ mA mm}^{-2}$ . Such inflection points are present in all curves for all ramping rates, yet the differences are more pronounced and appear for lower current densities for faster ramping rates. They are most likely explained by the incubation of a common thermal hot spot inside the sample, which is also indicated by the clearly heterogeneous microstructure between the bulk inside and the outer layer. No correlation could be established between the appearance of changes in power and the appearance of the steplike breakdown later.

Numerous sources have identified and investigated electrochemical reduction as a process during the incubation of flash sintering in various materials.<sup>[22–24]</sup> Further, both for flash sintering of strontium titanate and barium titanate, an increase in oxygen vacancies through doping has led to a lower onset of flash sintering.<sup>[25,26]</sup> Ren et al. investigated the incubation of the flash event in barium titanate from a standpoint of oxygen vacancy observations and concluded that oxygen vacancies accumulate during the incubation of the flash event until an avalanche breakdown transitions into the flash event.<sup>[27]</sup> Based on our data, both events take place, yet the breakdown is not causing the flash. As the solid platinum plate, electrodes are ultimately blocking atmospheric oxygen from reaching the center area of the sample directly, a disproportional amount of oxygen vacancies toward the center of the sample would provide an explanation for the breakdown. This also would explain why such dielectric breakdown appears at lower current densities for bulkier samples and, vice versa, why a bone-shaped sample can be fully densified

without experiencing such breakdown at all. However, due to the high mobility of oxygen vacancies against the timescale of the experiments (8–64 min), this cannot provide a satisfactory explanation. Yoshida et al. previously investigated the nature of damage in barium titanate after conventional flash experiments.<sup>[19]</sup> Based on the black colorization of the current path, also visible for our samples in Figure 4, they deduced a strong depletion of oxygen vacancies. In our case, such strong colorization only appears if the steplike dielectric breakdown appeared during the experiment. They concluded that the switching from *p*-type to *n*-type conductivity at elevated temperatures in barium titanate is responsible for the sudden current surge during conventional flash experiments and the coinciding dielectric breakdown. Both for strontium titanate and barium titanate, it is known that the conduction transitions from ionic to electronic for high temperatures.<sup>[28,29]</sup> This switching from ionic to electronic conduction after a transition point seems like a plausible explanation, yet it does not explain the dependence on the sample geometry we outlined or the ramping-rate dependent trend discussed earlier.

### 3. Conclusion

Ever since its introduction, controlled current ramping as a mode for flash sintering has been reported to significantly improve the results of flash sintering. Despite analogous reports of significant quality improvement for dog-bone-shaped barium titanate samples, we could not exceed a relative density of 85% for samples of only 6.5 mm diameter and 5.6 mm length, as samples experienced a critical steplike breakdown at values of only  $10 \text{ mA mm}^{-2}$ . As per our research, such breakdown appears to be a competing process to flash sintering of barium titanate, much rather than the cause for its incubation.

For conventional flash-sintering experiments, a regular thermal runaway preceded by a measurable thermal expansion of the samples could be verified for high fields.

Against the expectations based on the behavior of other oxides, the onset temperature of flash sintering in barium titanate does not converge to its Debye temperature.

### 4. Experimental Methods

Commercially obtained (Sigma Aldrich) barium titanate powder with a grain size of  $0.7 \mu\text{m}$  and a purity of >99% was used for all experiments. The green bodies were uniaxially pressed into cylindrical pellets at 50 MPa with a diameter of 6.5 mm and a height of 5.6 mm.

Controlled current ramping experiments were conducted at rates of 1, 0.5, 0.25, and  $0.125 \text{ mA s}^{-1}$  at a furnace temperature of 1000 °C up to a current density of  $15 \text{ mA mm}^{-2}$  (500 mA). Conventional flash experiments were conducted at a heating rate of  $10 \text{ K min}^{-1}$  for various electric fields up to  $1800 \text{ V cm}^{-1}$  (1000 V as the absolute upper potential difference limit).

The flash-sintering setup for this study was based on a Netsch DIL 402 Expedis dilatometer. For this setup, platinum electrodes with a diameter of 6.5 mm were co-pressed with the powder during the formation of the green body. No platinum paste was applied. The sample was oriented horizontally, with the pushrod of the dilatometer maintaining a constant 1 N force on the sample. Two configurations were used for the presented data: in the first configuration freeze-cast  $\text{Y}_2\text{O}_3$  insets of very low heat conductivity (heat conduction at 1000 °C:  $\lambda \approx 0.3 \text{ W m}^{-1} \text{ K}^{-1}$ ) with a diameter of 6.5 mm, a length of 5 mm, and a relative density of  $<1 \text{ g cm}^{-3}$  were

used as separators between the electrodes and the solid alumina parts of the setup. The detailed description of this material can be found elsewhere.<sup>[30]</sup> In the second configuration, the platinum wire (heat conductivity at 1000 °C:  $\lambda \approx 80 \text{ W m}^{-1} \text{ K}^{-1}$ ) was squeezed directly between the alumina parts of the dilatometer (at 1000 °C:  $\lambda \approx 8 \text{ W m}^{-1} \text{ K}^{-1}$ ) and the platinum electrodes together allowing for a strong thermal flow away from the samples.

A Keyence VHX digital microscope was used for high-resolution optical microscopy. A Philips XL 30 scanning electron microscope (SEM) was used for microstructure analysis.

Samples were cut down at the center parallel to field direction, which does not always include the dielectric breakdown path, and have been thermally etched at 1200 °C for 10 min.

## Supporting Information

Supporting Information is available from the Wiley Online Library or from the author.

## Acknowledgements

The authors are very grateful to the Deutsche Forschungsgemeinschaft (DFG) for supporting this project within the priority program SPP 1959 "Field Assisted Sintering" under grant no. Lu 729/25-1 (436254098). The authors gratefully acknowledge support by the Open Access Publication Fund of the University of Duisburg-Essen. The authors also thank V. V. Shvartsman of the University Duisburg-Essen for fruitful discussions.

Open Access funding enabled and organized by Projekt DEAL.

## Conflict of Interest

The authors declare no conflict of interest.

## Data Availability Statement

The data that support the findings of this study are available from the corresponding author upon reasonable request.

## Keywords

barium titanate, current ramping, Debye temperature, flash sintering, hot-spot formation

Received: January 30, 2023

Revised: April 12, 2023

Published online: May 5, 2023

[1] J. V. Campos, I. R. Lavagnini, J. G. Pereira da Silva, J. A. Ferreira, R. V. Sousa, R. Mücke, O. Guillon, E. M. J. A. Pallone, *Scr. Mater.* **2020**, 186, 1.

[2] M. Biesuz, V. M. Sglavo, *J. Eur. Ceram. Soc.* **2019**, 39, 115.

- [3] D. M. Hulbert, A. Anders, D. V. Dudina, J. Andersson, D. Jiang, C. Unuvar, U. Anselmi-Tamburini, E. J. Lavernia, A. K. Mukherjee, *J. Appl. Phys.* **2008**, 104, 033305.
- [4] C. Wang, W. Ping, Q. Bai, H. Cui, R. Hensleigh, R. Wang, A. H. Brozena, Z. Xu, J. Dai, Y. Pei, C. Zheng, G. Pastel, J. Gao, X. Wang, H. Wang, J.-C. Zhao, B. Yang, X. Zheng, J. Luo, Y. Mo, B. Dunn, L. Hu, *Science* **2020**, 368, 521.
- [5] L. Porz, M. Scherer, D. Huhn, L.-M. Heine, S. Britten, L. Rebohle, M. Neubert, M. Brown, P. Lascelles, R. Kitson, D. Rettenwander, L. Fulanovic, E. Bruder, P. Breckner, D. Isaia, T. Frömling, J. Rödel, W. Rheinheimer, *Mater. Horizons* **2022**, 9, 1717.
- [6] F. Trombin, R. Raj, *Am. Ceram. Soc. Bull.* **2014**, 93, 32.
- [7] T. P. Mishra, C. Lenser, R. Raj, O. Guillon, M. Bram, *J. Am. Ceram. Soc.* **2021**, 104, 4316.
- [8] Y. Nakagawa, H. Yoshida, A. Uehashi, T. Tokunaga, K. Sasaki, T. Yamamoto, *J. Am. Ceram. Soc.* **2017**, 100, 3843.
- [9] J.-C. M'Peko, J. S. C. Francis, R. Raj, *J. Eur. Ceram. Soc.* **2014**, 34, 3655.
- [10] M. Cologna, B. Rashkova, R. Raj, *J. Am. Ceram. Soc.* **2010**, 93, 3556.
- [11] S. López-Blanco, D. A. Ochoa, X. Vendrell, L. Mestres, J. E. García, *J. Eur. Ceram. Soc.* **2022**, 42, 5669.
- [12] A. Uehashi, H. Yoshida, T. Tokunaga, K. Sasaki, T. Yamamoto, *J. Ceram. Soc. Jpn.* **2015**, 123, 465.
- [13] D. Lewin, K. H. Menze, I. Michiels, D. C. Lupascu, *J. Eur. Ceram. Soc.* **2023**, 43, 1633.
- [14] H. Charalambous, S. K. Jha, K. H. Christian, R. T. Lay, T. Tsakalakos, *J. Eur. Ceram. Soc.* **2018**, 38, 3689.
- [15] M. K. P. Kumar, D. Yadav, J.-M. Lebrun, R. Raj, *J. Am. Ceram. Soc.* **2019**, 102, 823.
- [16] I. R. Lavagnini, J. V. Campos, J. A. Ferreira, E. M. J. A. Pallone, *J. Am. Ceram. Soc.* **2020**, 103, 3493.
- [17] X. L. Phuah, H. Wang, H. Charalambous, S. K. Jha, T. Tsakalakos, X. Zhang, H. Wang, *Scr. Mater.* **2019**, 162, 251.
- [18] T. P. Mishra, V. Avila, R. R. I. Neto, M. Bram, O. Guillon, R. Raj, *Scr. Mater.* **2019**, 170, 81.
- [19] H. Yoshida, A. Uehashi, T. Tokunaga, K. Sasaki, T. Yamamoto, *J. Ceram. Soc. Jpn.* **2016**, 124, 388.
- [20] S. Sanna, C. Thierfelder, S. Wippermann, T. P. Sinha, W. G. Schmidt, *Phys. Rev. B* **2011**, 83, 054112.
- [21] X. Meng, X. Wen, G. Qin, *Comput. Mater. Sci.* **2010**, 49, S372.
- [22] R. Kirchheim, *Solid State Ion.* **2018**, 320, 239.
- [23] T. P. Mishra, R. R. I. Neto, G. Speranza, A. Quaranta, V. M. Sglavo, R. Raj, O. Guillon, M. Bram, M. Biesuz, *Scr. Mater.* **2020**, 179, 55.
- [24] H. Zhou, X. Li, Y. Zhu, J. Liu, A. Wu, G. Ma, X. Wang, Z. Jia, L. Wang, *High Volt.* **2022**, 7, 1.
- [25] W. Rheinheimer, X. L. Phuah, H. Wang, F. Lemke, M. J. Hoffmann, H. Wang, *Acta Mater.* **2019**, 165, 398.
- [26] R. Shi, Y. Pu, J. Ji, J. Li, X. Guo, W. Wang, M. Yang, *Ceram. Int.* **2020**, 46, 12846.
- [27] K. Ren, S. Huang, Y. Cao, G. Shao, Y. Wang, *Scr. Mater.* **2020**, 186, 362.
- [28] R. A. De Souza, *Adv. Funct. Mater.* **2015**, 25, 6326.
- [29] C.-R. Song, H.-I. Yoo, *Solid State Ion.* **1999**, 120, 141.
- [30] E. Kröll, M. Vadalà, J. Schell, S. Stegemann, J. Ballof, S. Rothe, D. C. Lupascu, *Materials* **2021**, 14, 2864.